LA-UR- 10-01904

Approved for public release; distribution is unlimited.

Title:	Simulation Of Detonation Of Ammonium Nitrate Fuel Oil Mixture Confined By Aluminum: Edge Angles For DSD
Author(s):	Mark Short, James J. Quirk, Charles B. Kiyanda, Scott I. Jackson, Matthew E. Briggs, Micheal A. Shinas
Intended for:	14th International Detonation Symposium, Coeur d'Alene, Idaho, USA. April 11-16th 2010.

Los Alamos
NATIONAL LABORATORY
EST. 1943

Form 836 (7/06)

Simulation Of Detonation Of Ammonium Nitrate Fuel Oil Mixture Confined By Aluminum: Edge Angles For DSD

Mark Short[†], James. J. Quirk[†], Charles B. Kiyanda[†], Scott I. Jackson[†], Matthew E. Briggs[‡] & Micheal A. Shinas[‡]

[†]Shock and Detonation Physics Group, [‡]Hydrodynamic Experiments,
Los Alamos National Laboratory, Los Alamos, NM 87544

Abstract.
Non-ideal high explosives are typically porous, low-density materials with a low detonation velocity ($3 \sim 5$ km/s) and long detonation reaction zone ($\sim$ cms). As a result, the interaction of a non-ideal high explosive with an inert confiner can be markedly different than for a conventional high explosive. Issues arise, for example, with light stiff confiners where the confiner can drive the high explosive (HE) through a Prandtl-Meyer fan at the HE/confiner interface rather than the HE driving the confiner. For a non-ideal high explosive confined by a high sound speed inert such that the detonation velocity is lower than the inert sound speed, the flow is subsonic and thus shockless in the confiner. In such cases, the standard detonation shock dynamics methodology, which requires a positive edge-angle be specified at the HE/confiner interface in order that the detonation shape be divergent, cannot be directly utilized. In order to study how detonation shock dynamics can be utilized in such cases, numerical simulations of the detonation of ammonium nitrate-fuel oil (ANFO) confined by aluminum 6061 are conducted.

Introduction

Detonation Shock Dynamics (DSD) calculates the motion of a curved detonation through an explosive geometry; in its standard application, DSD requires knowledge of the detonation velocity variation as a function of surface curvature for a given explosive and the specification of an "edge angle" along the outer edge of the explosive that determines how the material (confinement) surrounding the explosive influences the detonation speed. For conventional or insensitive high explosives, like PBX 9501 or PBX 9502, a shock is transmitted into the confiner and the edge angle can be determined from a shock polar analysis at the explosive/confiner interface as described by Aslam and Bdzil[2, 3].

Non-ideal/home-made high explosives such as ammonium nitrate-fuel oil (ANFO) are typically porous, low-density materials with a low detonation velocity ($3 \sim 5$ km/s) and long detonation reaction zone (on the scale of centimeters rather than 100s of microns). As a result of these properties, the way a non-ideal high explosive interacts with the explosive confiner is markedly different than for a conventional high explosive. Significant issues arise, for example, with light stiff confiners where the confiner can now drive the high explosive (HE) through a Prandtl-Meyer fan at the HE/confiner interface rather than the HE driving the

confiner[2, 3]. The net effect is a negative edge angle at the HE/confiner interface for which the standard DSD capability cannot be utilized (which generally requires a positive edge-angle in order that the detonation shape be divergent). A simulation of this type of scenario where PBX 9502 is confined by a composite material was performed by Aslam & Bdzil[3]. In this case, it was observed that the region where the detonation shock is convergent is confined to a narrow layer adjacent the confiner. Aslam & Bdzil[2, 3] have discussed the shock polar analysis at the HE/confiner interface for most cases relevant to conventional and non-ideal HE.

For a conventional or non-ideal HE confined by a high sound speed inert such that the detonation velocity is lower than the sound speed in the inert, there is no possible shock polar match. The flow is subsonic and thus shockless in the confiner. Eden and Wright[6] examined the wave shape in a brass/Baratol/Al and a brass/Comp. B/beryllium sandwich test configuration. For the brass/Baratol/Al configuration, they observed a precursor elastic wave running at the Al sound speed, followed by a weak shock in the Al just ahead of the detonation, causing the interface to precompress undetonated HE. The detonation velocity at the Baratol/Al interface was $\sim$ 5% greater than the normal plane speed in Baratol. Similarly, Eden and Belcher[5] examined the detonation of a brass/EDC35/beryllium sandwich configuration (25 mm EDC35, 9.3mm beryllium and 10mm brass thicknesses). A precursor elastic wave in the beryllium was followed by a beryllium shock ahead of detonation. The velocity of detonation was enhanced by $\sim$ 1%. Eden and Belcher[5] attribute this to a thin layer of undetonated EDC35 preshocked before the detonation front reaches it. Tarver & Mcguire[10] conducted an ignition and growth model simulation of Eden and Belcher[5], finding that the global features observed experimentally are captured by the simulation. A simulation of 40 mm heavy ANFO confined by 49 mm steel Clark Souers *et al.*[4] reveals a steel precursor wave ahead of the detonation that drives the inner wall into the HE causing the explosive to pre-initiate. Sharpe and Bdzil[8] examined analytically the effect on detonation of subsonic flow in the inert when the overall change in the sound speed of the inert is small. The subsonic flow deflects the interface toward explosive. For sufficiently thick inerts, deflection of the confiner should drive the detonation speed in the explosive up to sound speed of the inert and/or drive a precursor wave ahead of detonation in explosive. A simulation of an emulsion explosive confined by hard rock where the thickness of the HE was equal to that of the inert was conducted by Sharpe *et al.*[9].

In regard to the effect of confinement on detonation propagation when the detonation velocity is lower than the sound speed in the inert, it appears that a number of competing mechanisms are present. Energy transferred into the confiner from the detonating HE can propagate upstream of the detonation shock. The energy propagated upstream can drive the confiner surface into the HE, changing the confinement conditions; the detonation velocity can be significantly increased beyond that one would expect with no upstream energy transfer; alternatively, for porous non-ideal HE, the collapse of the heterogeneous pores due to the upstream energy transfer can lead to local failure of the detonation due to absence of hot-spot generation; in some cases, the energy transfer can cause upstream fracture of the confining material leading to the disappearance of confinement which in turn can result in detonation failure, as observed experimentally[1]. The nature of the HE/confiner interaction in such cases is determined by the confiner sound speed, its density and thickness.

In order to develop a DSD capability for configurations in which the detonation velocity is lower than the sound speed of the confiner, further understanding of the physics of this process is necessary. In this article, we present numerical simulations of the detonation of ANFO confined by aluminum 6061

ANFO-Al rate-stick: PDV diagnostics

A series of rate-stick experiments on the effect of aluminum confinement on the behavior and shape of ANFO (94/6 wt.% AN/F0) detonation have been conducted for varying Al wall thicknesses[7]. On one configuration (shown in fig. 1), four focused photon doppler velocimetry (PDV) probes were placed along the axis of the tube, with a 50 mm wall stand-off distance (in addition, four collimated PDV probes were placed along an axis of the end of tube,

Fig. 1. Set-up of cylindrical Al confinement of ANFO (94/6 wt.% AN/FO). The ANFO/Al tube length was 914.4 mm. The ANFO ID was 76.2 mm, while the Al wall thickness was 12.7 mm.

again with a 50 mm stand-off distance). Along the tube axis, the PDV probes were aligned with the axial position of shorting, ionization and piezo pins.

The detonation velocity was 3.466 mm/μs. A precursor elastic wave running at 5.09 mm/μs in the Al was detected by a signal in the piezo pins. Figure 2 shows the velocity of the outer wall expansion in the radial direction detected by axial PDV probes PDV2 (33.1851 cm from the tube end wall) and PDV3 (8.5217 cm from the tube end wall). The elastic precursor causes an oscillatory wall motion with induced velocities of the order of 5 m/s (since an acoustic-optic frequency shifter was not employed, it is difficult to ascertain whether the radial wall motion changes direction, or simply accelerates and decelerates). More significantly, both PDV2 and PDV3 records show a more rapid but continuous expansion of the wall lasting of the order of 2 μs, prior to a more dramatic increase in the wall velocity (presumably corresponding to the detonation arrival). For the PDV3 record, it appears that the precursor pressure disturbance immediately ahead of the detonation causes the wall to accelerate out radially and then decelerate prior to detonation arrival. For a detonation progressing at 3.466 mm/μs, a 2 μs pressure disturbance period ahead of the detonation is equivalent to an approximately 7 mm spatial region.

Figure 3 show the shorting, ionization and piezo

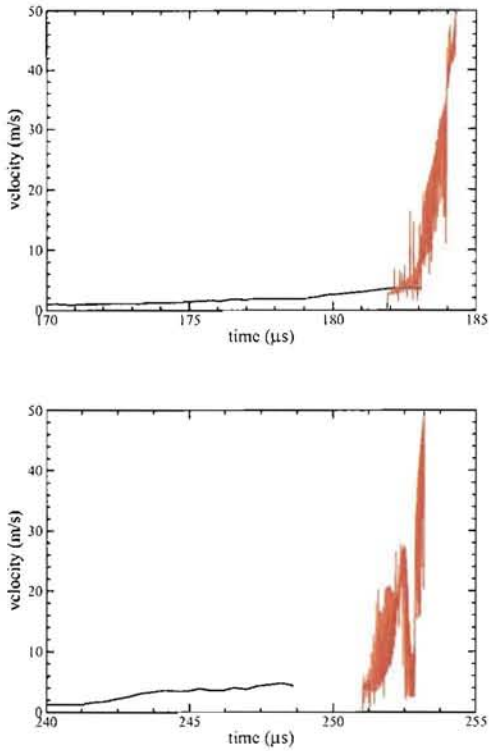

Fig. 2. Al outer wall motion detected by PDV probes 2 (PDV2, top figure) and 3 (PDV3, lower figure), located 331.851 mm and 85.217 from the tube end respectively.

pin signal records corresponding to the locations of PDV2 and PDV3. In particular, the piezo records also indicate the arrival of a smooth precursor pressure wave just prior to the arrival of detonation. The time period of the precursor pressure wave is $\sim$ 1 μs.

Figure 4 (record d) shows the detonation front shape for set-up described in fig. 1[7]. The record is smeared due to a separation between the ANFO and a PMMA window (with a PETN paint strip designed to illuminate the detonation break out) at the end of the tube as described by Jackson, Kiyanda and Short[7]. Also shown is a sharper record obtained from a 305 mm long Al tube with an inner ANFO diameter of 76.2 mm and a 25.4 mm thick Al wall (record e). In both cases, a flattening of the wave

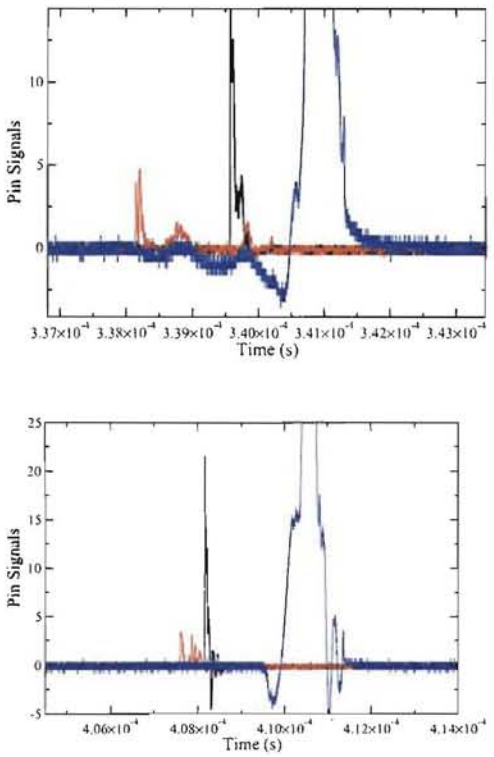

Fig. 3. Shorting (red lines), ionization (black lines) and piezo pin (blue lines) signal records at the PDV2 (top figure) PDV3 (bottom figure) locations.

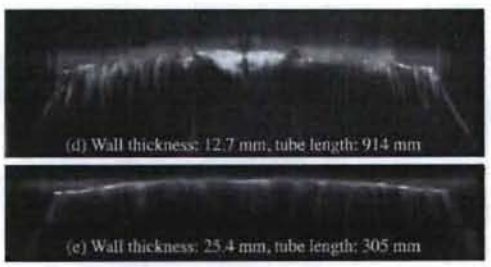

Fig. 4. Streak camera detonation front record. Record (d) corresponds to fig. 1, while record (e) is for a 305 mm long tube, ANFO diameter of 76.2 mm, with a 25.4 mm Al thick wall.

can be observed near the wall, with the curvature of the front reaching a maximum in the interior of the ANFO. It is difficult to isolate an explicit upturn of the wave at the boundary from these images as predicted by theory.

Model

Our reactive flow model for ANFO consists of a two-component mixture of reactants and products. The initial density of the material is $\rho_0 = 1/v_0 = 0.88$ g/cc. A JWL based EOS is used for the products, with an internal energy e given by

$$e_g = \frac{v_g}{\omega}\left[p_g - A\left(1 - \frac{\omega v_0}{R_1 v_g}\right)\exp(-R_1 v_g/v_0) - B\left(1 - \frac{\omega v_0}{R_2 v_g}\right)\exp(-R_2 v_g/v_0)\right], \quad (1)$$

for pressure p and specific volume v. The subscript $\{\}_g$ is used to denote the product state. The parameters A, B, R_1, R_2 and ω (constant Gruneisen Gamma) are given by

$$A = 1.049\ g/cm\ \mu s^2,\ B = 0.01623\ g/cm\ \mu s^2, \quad R_1 = 4.658,\ R_2 = 1.138,\ \omega = 0.2916, \quad (2)$$

from an ANFO calibration given by Wescott[11]. For the ANFO reactants EOS, we use a Mie-Gruneisen EOS based off a linear $U_s - u_p$ fit to reactant Hugoniot data[11]. Specifically, with

$$U_s = \hat{c} + su \quad (3)$$

then,

$$e_s = e_{sh} + \frac{v_0}{\Gamma_0}(p_s - p_{sh}) \quad (4)$$

where the shock Hugoniot variations are,

$$p_{sh} = \frac{\hat{c}^2(1 - v_s/v_0)}{v_0[1 - s(1 - v_s/v_0)]^2}, \quad e_{sh} = \frac{\hat{c}^2(1 - v_s/v_0)^2}{2[1 - s(1 - v_s/v_0)]^2}. \quad (5)$$

The subscript $\{\}_s$ is used to denote the reactant state. The calibrated parameters $\hat{c}$, s and Γ_0 are again taken from Wescott[11] as,

$$\hat{c} = 0.0977 cm/\mu s,\ s = 1.42,\ \Gamma_0 = 0.967. \quad (6)$$

The closure conditions for the mixture are:

$$p = p_s = p_g,\ v = (1-\lambda)v_s + \lambda v_g,$$
$$e = (1-\lambda)e_s + \lambda e_g - \lambda e_0, \tag{7}$$

along with an assumption that the post-shock entropy S in the solid is fixed,

$$\frac{DS_s}{Dt} = 0. \tag{8}$$

The heat release e_0 (the energy of the initial state relative to the products on the CJ isentrope at $\rho = 0$ and temperature $T = 0$) is given by

$$e_0 = 4.3434 \times 10^{-2}\ cm^2/\mu s^2. \tag{9}$$

With this calibration, the CJ state of the one-dimensional steady ANFO detonation is calculated to be,

$$D_{CJ} = 0.48006\ cm/\mu s,\ v_{CJ} = 0.8174\ cc/g,$$
$$p_{CJ} = 0.05695\ g/cm\ \mu s^2. \tag{10}$$

We implement a one-step reaction between reactants and products with a pressure dependent reaction rate given by

$$r_s = k_s p^{n_s}(1-\lambda)^{\nu_s}, \tag{11}$$

where

$$n_s = 2,\ \nu_s = 1,\ k_s = 200\ g/cm\ \mu s^3. \tag{12}$$

For the aluminum confinement, we again use a linear $U_s - u_p$ EOS with

$$U_s = \hat{c}_{Al} + s_{Al}u. \tag{13}$$

For aluminum, the calibration parameters are

$$\hat{c}_{Al} = 0.5328\ cm/\mu s.\ s_{Al} = 1.338,$$
$$\Gamma_{0Al} = 2,\ v_{0Al} = 1/2.70\ cc/g. \tag{14}$$

Polar Analysis

Figure. 5 shows the shock polar behavior for the ANFO reactant EOS given by (3-6), and the Al EOS given by (13-14) for non-oblique shock velocities 6 mm/μs, 7 mm/μs and 8 mm/μs. In all cases, the maximum turning angle for the ANFO polar is significantly greater than for the Al polar. The detonation velocity of ANFO varies in particular with prill density and size. For 8 mm/μs, there are two intersection points; one corresponding to strong confinement having subsonic flow in both the ANFO and Al. The other corresponds to a non-traditional shock interaction case, where the polars are connected via a Prandtl Meyer fan originating at the Al sonic point, so that the Al is driving the ANFO locally. Sandwich test cases of this nature have been examined numerically by Aslam and Bdzil[2, 3] (see also Sharpe *et al.*[9]). It was found that the detonation front turns up toward the confiner in a narrow region near the HE/confiner interface, i.e. becomes locally convergent. Since the match of the Prandtl Meyer fan is on the supersonic portion of the HE polar, a local region of supersonic flow must exist in the HE near the confiner interface. At 7 mm/μs, the Al polar lies completely within the ANFO polar, and the only solution is a Prandtl Meyer fan originating at the Al sonic point and intersecting the ANFO polar. For 6 mm/μ,s the ANFO intersection point of a Prandtl Meyer fan from the Al polar would be at a low pressure that is not likely physically relevant[8]. For a shock velocity lower than the sound speed in the Al, no shock polar exists for the Al, and thus no shock polar match is possible.

Simulation

We have performed a simulation of ANFO confined by Al in a two-dimensional symmetric sandwich test configuration. The total thickness of the ANFO is 7.62 cm, while the thickness of the Al is 2.54cm. The simulation is performed with the AMRITA environment, which provides a state-of-the-art capability for multi-material, adaptive-mesh refined simulation of high explosive applications. The reactive flow model uses the ANFO system (1-6) and the Al system (13-14) with closure conditions (7-8). The flow updates in the ANFO and Al are obtained with a three-stage TVD Runge-Kutta integration using a Lax-Friedrichs flux with WENO reconstruction. The ANFO/Al material boundary uses a ghost fluid approach with linearized Riemann solver coupling. The pressure and velocity come directly from the Riemann solution, while the density uses half the expected jump. Outflow extrapolation conditions are used on the top Al boundary, outflow extrapolation conditions are used at the left and right hand side boundaries, while symmetry conditions

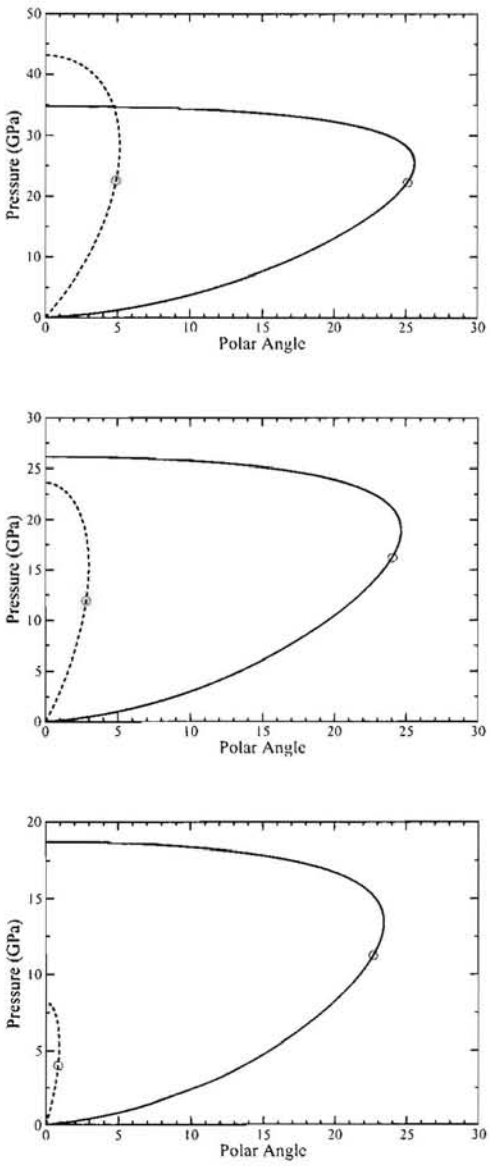

Fig. 5. Shock polars for the ANFO reactant EOS (solid lines) given by (3-6) and the Al EOS (dashed lines) given by (13-14). The non-oblique shock speeds in each case are (a) 8 mm/μs (top figure), (b) 7 mm/μs (middle figure) and (c) 6 mm/μs (bottom figure). The circles indicate sonic flow on each branch.

are used on the lower HE boundaries. The initial state in the ANFO corresponds to a ZND detonation wave solution placed near the left hand boundary. The upstream state in the ANFO is quiescent. The initial state in the Al is quiescent.

Figure 6 shows a sequence of pressure contours (based on 20 equal increments from the pressure maximum to the pressure minimum) at times $t = 25.58\ \mu s$, $t = 66.80\ \mu s$ and $t = 127.4\ \mu s$. Corresponding pseudo-Schlieren images are shown in figure 7. Also shown in figure 7 are surfaces in the ANFO representing 50% and 99% reactant depletion. The high pressure flow behind the initial ZND wave in the ANFO drives the ANFO/Al interface outward initially. The high sound speed in the Al causes a pressure pulse to develop ahead of the detonation front, and at $t = 25.58\ \mu s$, the development of the precursor pressure wave is prominant. The deflection of the interface at $t = 25.58\ \mu s$ is weak, and no significant curvature in the detonation wave has developed. At $t = 66.80\ \mu s$, the pressure pulse in the Al continues to drive the detonation. The corresponding Schlieren image indictates that a region of the detonation shock near the interface has become convergent. At $t = 127.4\ \mu s$, the detonation front is completely convergent. The precursor wave in the Al is sufficiently driving the detonation in the ANFO that the curvature is negative. The surface of 50% reactant depletion is also convergent, while the surface of 99% reactant depletion again becomes divergent in a small region near the interface. There is also a density and pressure flow gradient ahead of the detonation front in the ANFO, a result of the precursor pressure wave in the Al compressing the ANFO. Of particular interest is the behavior of the ANFO/Al interface at late times. The Al wall expands slightly into the ANFO in the precursor pressure region[8], and increasingly expands into the ANFO during the passage of the ZND wave and for a significant portion of following product flow. Subsequently, the high pressure of the product flow begins to drive the wall motion outward.

The results here are somewhat different from those described in the PDV experiment described above. As determined by Aslam & Bdzil[2, 3] and Sharpe and Bdzil[8] the nature of the HE/confiner interaction is determined by the confiner sound speed,

its density and thickness relative to those of the HE. An analysis of the detonation wave shape in figures 6 and 7 should be carried out to determined how to apply detonation shock dynamics to such cases.

References

1. Arai, H. , Ogata, Y. , Wada, Y. , Miyake, A. , Jung, W. J. , Nakamura, J. , and Ogawa, T. . Detonation behavior of ANFO in resin tubes. *Sci. Technol. Energetic Mat.*, 65:201–205, 2004.

2. Aslam, T. D. and Bdzil, J. B. . Numerical and theoretical investigation on detonation-inert confinement interactions. In *Proceedings of the 12th Symposium (International) Detonation*, pages 483–88. ONR 333-05-2, 2002.

3. Aslam, T. D. and Bdzil, J. B. . Numerical and theoretical investigations on detonation confinement sandwich tests. In *Proceedings of the 13th Symposium (International) on Detonation*, pages 761–769. ONR 113291-7, 2006.

4. Clark Souers, P. , Vitello, P. , Esen, S. , Kruttschnitt, J. , and Bilgin, H. A. . The effects of containment on detonation velocity. *Propell. Explos. Pyro.*, 29:19–26, 2004.

5. Eden, G. and Belcher, R. A. . The effects of inert walls on the velocity of detonation in EDC35, An Insensitive High Explosive. In *Proceedings of the 9th Symposium (International) Detonation*, pages 831–841. ONR 113291-7, 1989.

6. Eden, G. and Wright, P. W. . A techninque for the precise measurement of the motion of a plane free surface. In *Proceedings of the 4th Symposium (International) Detonation*, pages 573–583. ONR ACR-126, 1965.

7. Jackson, S. I. , Kiyanda, C. B. , and Short, M. . Precursor detonation wave development in ANFO due to aluminum confinement. In *These Proceedings*, 2009.

8. Sharpe, G. J. and Bdzil, J. B. . Interaction of inert confiners with explosives. *J. Eng. Math.*, 54:273–98, 2006.

9. Sharpe, G. J. , Luheshi, M. Y. , Braithwaite, M. , and Falle, S. A. E. G. . Steady non-ideal detonation. In Elert, M. L. , Butler, W. T. , Furnish, M. D. , Anderson, W. W. , and Proud, W. G. , editors, *Shock Compression of Condensed Matter*, pages 452–457. AIP, 2009.

10. Tarver, C. M. and McGuire, E. M. . Reactive Flow Modeling of the Interaction of TATB Detonation Waves with Inert Materials. In *Proceedings of the 12th Symposium (International) Detonation*, pages 641–649. ONR 333-05-2, 2002.

11. Wescott, B. L. . Generalized pseudo-reaction zone model for non-ideal explosives. In Elert, M. , Furnish, M. D. , Chau, R. , Holmes, N. , and Nguyen, J. , editors, *Shock Compression of Condensed Matter*, pages 433–436. AIP, 2007.

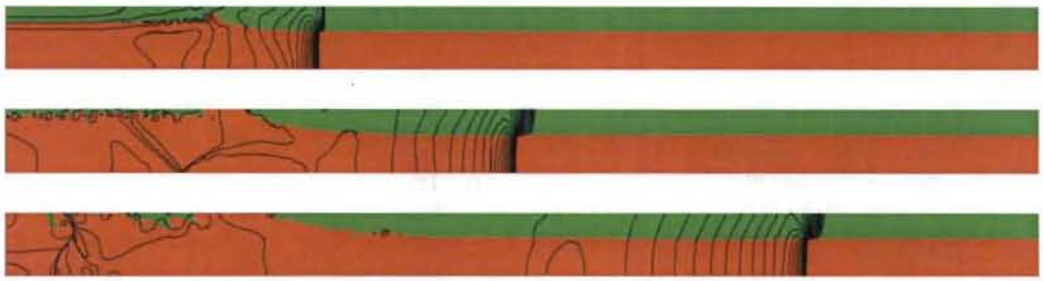

Fig. 6. Pressure contours at time $t = 25.58\ \mu s$ (top figure), $t = 66.80\ \mu s$ (middle figure) and $t = 127.4 \mu s$ (bottom figure). The contours are plotted based on 20 equal increments from the pressure maximum to the pressure minimum. Red coloring corresponds to ANFO region, while green corresponds to Al.

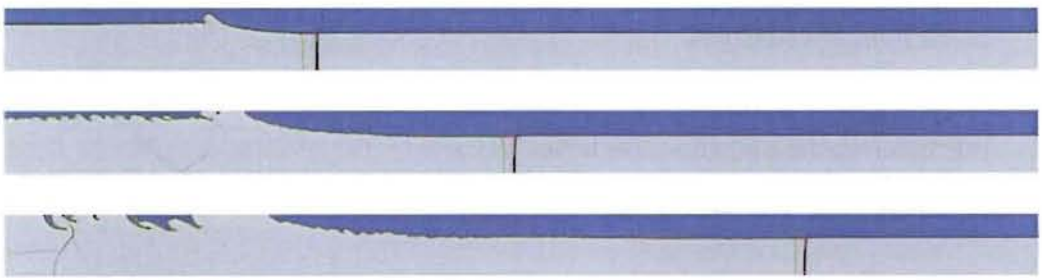

Fig. 7. Pseudo-Schlieren images at time $t = 25.58\ \mu s$ (top figure), $t = 66.80\ \mu s$ (middle figure) and $t = 127.4\ \mu s$ (bottom figure). Blue coloring corresponds to ANFO region, while grey corresponds to Al. The red line corresponds to 50% reactant depletion, while the green line corresponds to 99% reactant depletion.